

Blood flow and damage by the roller pumps during cardiopulmonary bypass

J.W. Mulholland^{a,b}, J.C. Shelton^b, X.Y. Luo^{c,*}

^aLondon Perfusion Science, Clinical Perfusion, London Independent Hospital, 1 Beaumont Square, Stepney Green, London E1 4NL, UK

^bDepartment of Engineering, Medical Engineering Division, Queen Mary, University of London, London E1 4NS, UK

^cDepartment of Mechanical Engineering, University of Sheffield, Mappin Street, Sheffield S1 3JD, UK

Received 8 October 2002; accepted 6 October 2004

Abstract

Although much CFD work has been carried out to study the blood damage created in a centrifugal pump used for a cardiopulmonary bypass, little is known about the blood flow and consequent damage in a roller pump. A time-dependent moving boundary problem is solved in this paper to explore the blood flow and damage in the roller pump. An initial attempt to predict the blood damage from these simulations is also made and results are compared with experimental observations. It is discovered that reducing the amount of time two rollers simultaneously occlude the tubing, will reduce the blood exposure to shear stress significantly and consequently reduce the blood damage caused. © 2004 Elsevier Ltd. All rights reserved.

1. Introduction

During open-heart surgery, cardiopulmonary bypass (CPB) is used to isolate the heart and lungs from the remainder of the circulation. The primary function of the heart and lungs is the provision of blood circulation, to provide oxygen and other nutrients to the cells and to remove the products of metabolism. These functions are therefore undertaken by the CPB system. The blood gas exchange device (oxygenator) performs the function of the lung by adding oxygen to the blood whilst carbon dioxide is removed. During CPB the venous return to the right heart is diverted via a cannula by syphonage to the venous reservoir of the CPB system. The venous reservoir has two roles. It acts as a capacitance chamber, which allows for variations in the patient's circulating volume, and it also filters the blood removing air and other embolic material. A roller, or centrifugal pump, the analogue of the left ventricle, sucks blood from the reservoir and pumps it through the heat exchanger and the oxygenator. Blood that spills into the open chest cavity is returned to the systemic system via a low-pressure suction system which is driven by a separate roller pump.

It is well established that CPB damages the blood (Mulholland et al., 2000; Yarbrough et al., 1966) by subjecting it to non-physiological forces (Blackshear et al., 1965; Nevaril et al., 1968; Leverette et al., 1972; Williams, 1973; Bernstein et al., 1967; Bluestein and Mockros, 1969), therefore prolonging the patient's recovery. A great deal of research has been focused on reducing this damage. Many major advances in CPB have been achieved, for example oxygenators are more efficient, the materials used are more biocompatible and the circuits are therefore safer. Nevertheless, it has become

*Corresponding author. Tel.: +44 114 2227752; fax: +44 114 2227890.

E-mail addresses: John@londonperfusionscience.com (J.W. Mulholland), J.Shelton@qmul.ac.uk (J.C. Shelton), X.Y.Luo@sheffield.ac.uk (X.Y. Luo).

important to reconsider some of the more detailed aspects of the current system in terms of the precise nature of the damage to the blood cells. Improving the way blood flows through the circuit is a key area for the advancement of CPB. The geometry of the circuit will influence the fluid dynamics in the system and therefore how the blood is handled. Detrimental flow structures such as areas of turbulence, stagnation, vortices, recirculation, high shear stresses, and negative pressure all contribute to increased blood damage (Mulholland et al., 2000).

One of the key areas of the CPB circuit is the arterial pump, which provides the blood with momentum. There are two types of pump currently used, the roller pump (peristaltic) and the centrifugal pump (constrained vortex). It was believed when the centrifugal pump was introduced into the CPB circuit, as the arterial pump, that their evolution would eventually render the roller pump obsolete. With recent independent research failing to show any advantage of using a centrifugal pump over a roller pump (Hansbro et al., 1999; Takahama et al., 1985) for short-term assist (less than 8 h), perfusionists continue to use roller pumps as the arterial pump as they are simple and cost effective. The initial expectations of the centrifugal pump led to a considerable amount of numerical simulation (Anderson et al., 2000; Bludszweit, 1995a; Sukumar et al., 1996; Nakamura et al., 1999; Huang and Fabisiak, 1978; Miyazoe et al., 1998, 1999; Takiura et al., 1998) being carried out on this device. There has been little published literature investigating the roller pump during the past 20 years. This paper presents a two-dimensional numerical simulation of a roller pump. The aims were to understand the detailed fluid dynamics of the roller pump and assess the potential of using the CFD results in a theoretical blood damage prediction model. In order to accurately understand blood flow in a roller pump it was necessary to perform a time-dependent flow simulation with a deforming mesh. The detailed flow patterns, as well as shear stress in the flow were examined. Although this is a two dimensional approach, it provides the first step towards a more realistic model. These results will be used to identify the deficiencies of the current designs for roller pumps from a fluid dynamic point of view. The hypothesis was set that if an accurate model of the roller pump could be generated using CFD it would be possible to refine the design more easily and thereby reduce the amount of blood damage caused.

2. The model

2.1. The geometry

A two-dimensional model of the system was obtained using an established protocol that combined computer-aided drawings, a digital camera and digitization of these images (Fig. 1). The digital camera was positioned over the central point of the roller pump using a plumb line and a spirit level. The silicon roller pump boot is shown in Fig. 1. It lies along the wall of the pump housing, and is compressed by the rollers providing peristaltic flow. Images of the roller pump boot were taken at every degree between $\theta = 0^\circ$ and 180° in order to establish the changes in geometry. The pump boot was filled with black dye making the inner edges clearly definable.

Occlusion of the roller pump, i.e. the distance between the inner walls of the pump boot at the point of roller contact was set to be *just* under occlusive using a qualitative, clinically established protocol (London Independent Clinical Protocols, 1994). The rollers are manually tightened to be fully occlusive using the pumps integrated control. The outlet of the pump boot is clamped off and the roller is turned to generate a positive pressure of 280 mmHg ensuring the leading roller is positioned at $\theta = 90^\circ$. The pressure is measured at the outlet of the pump boot using a Tyco pressure gauge that is an integrated part of the CPB tubing circuit. The roller occlusion is then loosened until the pressure decreases at a rate of 1 mmHg/s. Using the same method the occlusion of both rollers are checked with the leading roller at $\theta = 0^\circ, 45^\circ$ and 135° . The protocol has been designed to minimize the back-flow caused by significant under-occlusion whilst avoiding cell crushing caused by over-occlusion. The geometry acquisition technique showed that with the occlusion set correctly, the gap between the inner walls at the point of roller contact was 1 mm.

2.2. Governing equations

The Navier–Stokes equations are given below, where ρ is the fluid density, u_i is the velocity component in the x_i direction ($i = 1, 2$), p is the pressure, τ_{ij} is the stress tensor, and repeated indices are summed:

$$\frac{\partial u_i}{\partial x_i} = 0, \quad (1)$$

$$\rho \left[\left(\frac{\partial u_i}{\partial t} \right) + \frac{\partial}{\partial x_j} (u_i u_j) \right] = - \frac{\partial p}{\partial x_i} + \frac{\partial \tau_{ij}}{\partial x_j}. \quad (2)$$

These are solved using a commercial CFD package Fluent 4.

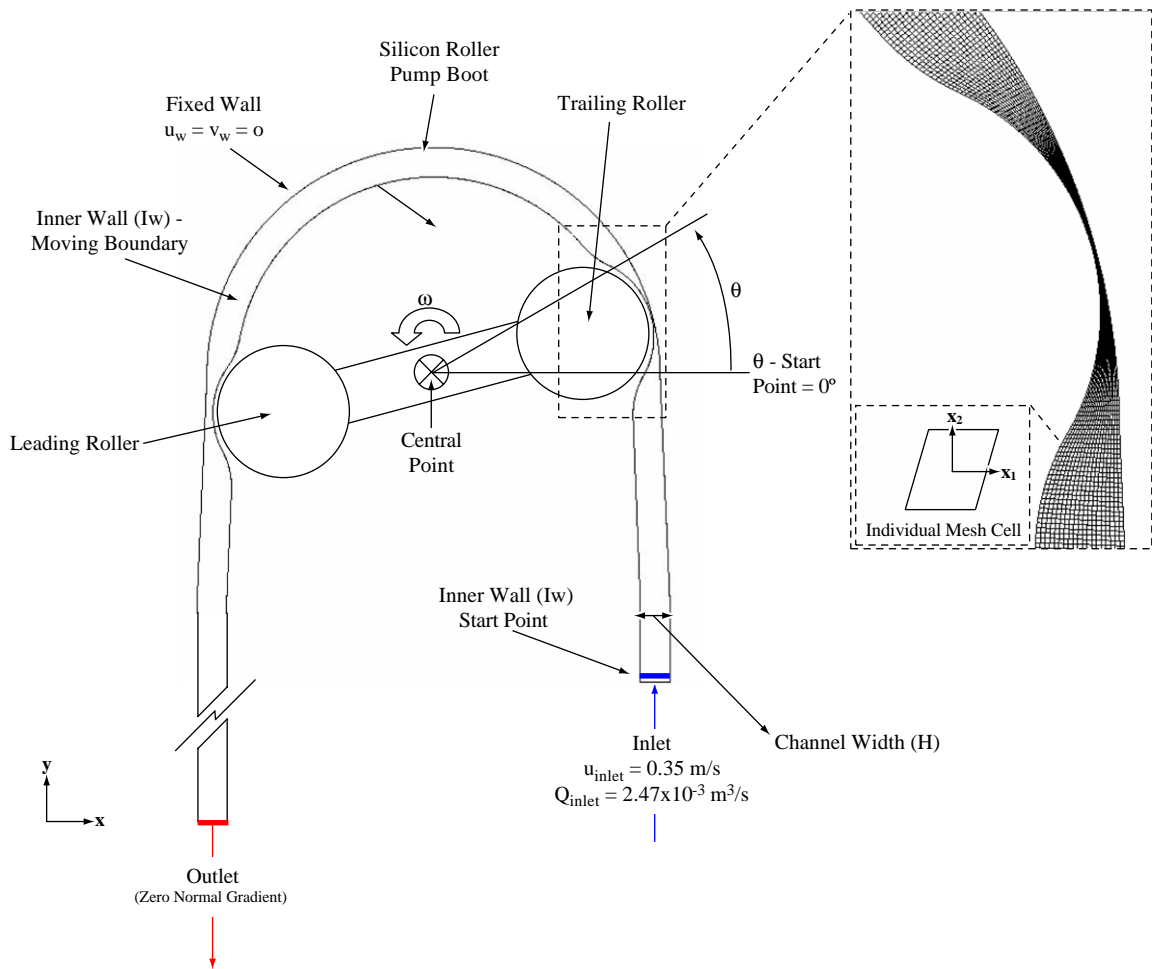


Fig. 1. The geometry, boundary conditions and meshing of the roller pump boot.

Blood was modelled as Newtonian, with a constant density of 1050 kg/m^3 and a constant viscosity of $3.5 \times 10^{-3} \text{ kg/m s}$. The Casson plot (Fung, 1993) showed that blood demonstrates non-Newtonian properties at low shear rates (less than 100 s^{-1}), whilst above this threshold shear rate blood exhibits Newtonian properties. These findings were confirmed by Huang and Fabisiak (1978), and Bludszweit (1995a), who both showed that at higher shear rates blood can be modelled as Newtonian. This assumption of Newtonian behaviour holds for the shear rates found in this simulation.

2.3. Initial and boundary conditions

2.3.1. Initial conditions

As the initial conditions are themselves a solution of the system at the end of each cycle, one of the early simulations was run for five revolutions. It was found that the results stabilized and began repeating every 180° after 540° ($1\frac{1}{2}$ revolutions). The results data file at $\theta = 540^\circ$ was used to supply the initial conditions for the final case file.

2.3.2. Boundary conditions

The boundaries of the model consisted of an inlet, an outlet, a no-slip wall boundary, and a moving boundary (see Fig. 1). The flow rate was measured to be $2.47 \times 10^{-5} \text{ m}^3/\text{s}$, which corresponded to an inlet velocity of 0.35 m/s , giving a Reynolds number $Re = \rho u_{inlet} H / \mu = 496$. A parabolic velocity profile was used at the inlet, and zero pressure was specified at the outlet. The velocity at the stationary and moving walls of the pump boot satisfied the no-slip condition.

3. Methods

The simulation was time dependent and the shape of the pump boot changed with time. This shape is associated with the periodic passage of the rollers.

3.1. The time-dependent model

To solve this time-dependent moving boundary problem, the model was set to automatically save the data files every 5 time steps (0.5°). The time-dependent and deforming mesh models were used at each time step to describe the grid deformation with interpolation between files. The time-dependent equations were solved using an implicit formulation, requiring iteration at each time step, and the maximum number of iterations per time step was set to 100. The minimum residual sum was set to 10^{-3} . Convergence was achieved when the sum of the absolute values of normalized residuals was less than this value. The number of time steps between each grid file was set to 10, thereby determining the size of the time step Δt as 3.44×10^{-4} s, which was the time taken for the roller to travel 0.1° .

3.2. The computational methods and the deforming mesh model

At each time step, the model was solved using a power law discretization scheme, which provides a formal accuracy between 1st and 2nd order schemes. The components of the velocity were updated using a line Gauss–Seidel equation solver, which was set to sweep in a direction normal to the primary direction of flow. In order to speed the convergence of the standard line solver, a multigrid scheme was used to solve the pressure correction equations.

As the grid topology must not change throughout the calculation, it was important that the deformation of the mesh should not proceed to the extent that a skewed mesh was generated. This would produce inaccurate results and was therefore carefully considered during the initial mesh generation.

A summary of the method used to generate the CFD model of the roller pump is shown in Fig. 2. A geometry file was created for each degree throughout the rotation. The size and topology of the mesh was determined from a single geometry file.

4. Code validation

Finding the optimum grid size and the optimum time step were important to ensure that accurate results were obtained using the minimum amount of computer memory and time. The method that was used to determine these values involved changing the size of each parameter in turn. The size of the mesh was increased while the time step was reduced. The model was initially meshed (2136 cells—angular interval = 0.81°) and modeled under the steady state condition when two rollers are in the position of $\theta = 0$. The mesh size was increased to 6886 cells (angular interval = 0.42°) and the analysis carried out again. This process was repeated until the difference in maximum vorticity between the two sets of results was less than 1%. The mesh at this point had 21,639 cells (angular interval = 0.26°), and was taken to be the optimum grid size.

This mesh was then incorporated into a time-dependent case file along with the boundary conditions and the deforming mesh model. The model was initially run with a 1.13×10^{-3} s (1°) time step; the time step was then reduced to 5.67×10^{-4} s (0.5°). This process was also repeated until the difference in maximum vorticity between the two sets of results was less than 1%. The optimal time step was found to be 3.44×10^{-4} s (0.3°).

5. Results

5.1. Velocity fields

Due to the large amount of data produced in this time-dependent simulation, only velocity magnitude contours are shown for selected parts of the flow domain at selected times. However, the observations we made also included flow information not shown here.

The velocity magnitude contours of the flow near the rollers at various roller positions from $\theta = 0^\circ$ to 180° are shown in Figs. 3(a)–(e). The scales are not the same for each figure, as this would result in poor velocity contour distinction in individual plots. At $\theta = 0^\circ$, both the leading roller (grey) and the trailing roller (white) are occluding the tube. The maximum velocity occurs at the narrowest part of the tube and is as high as 11.31 m/s, since the gap between the roller

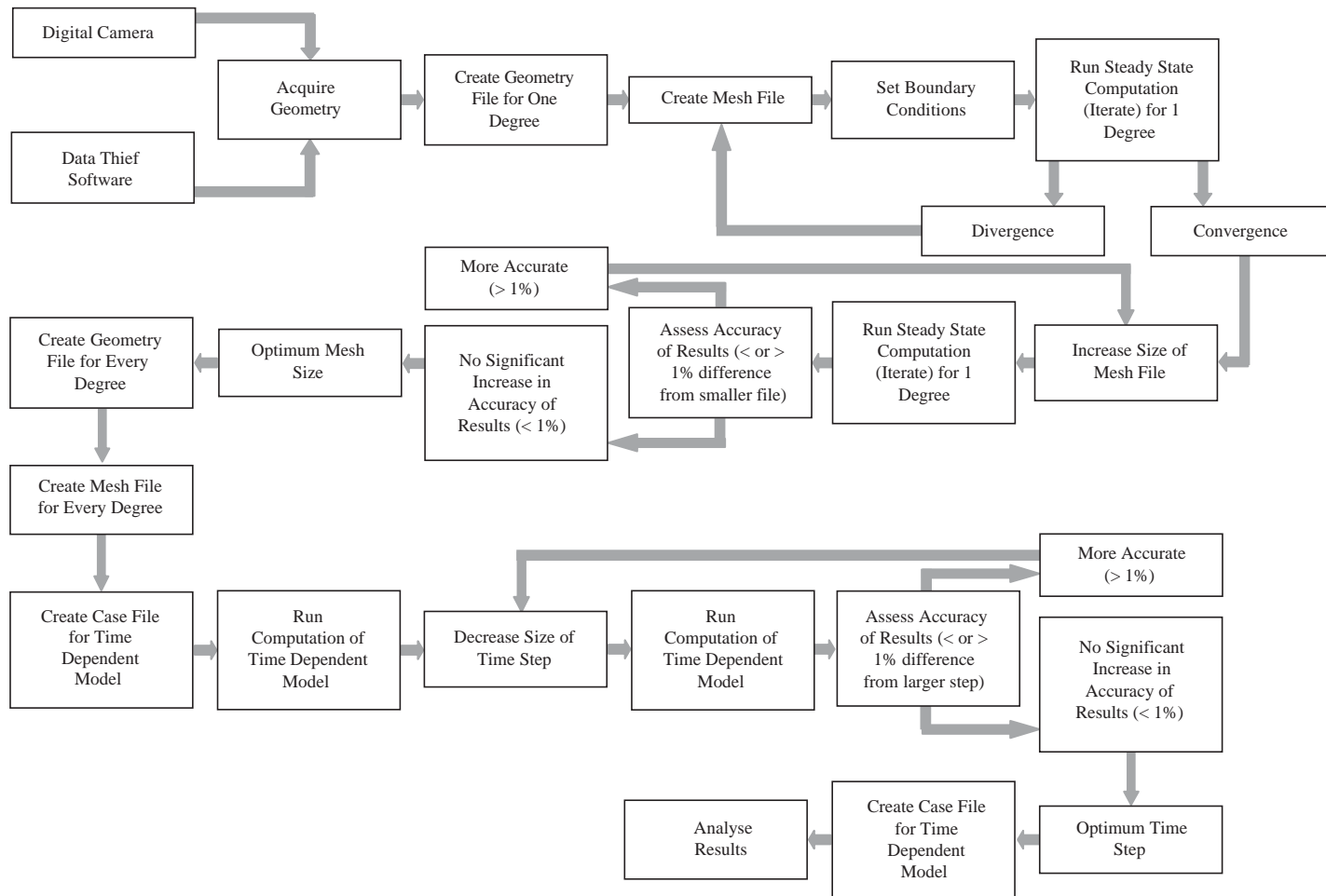


Fig. 2. Flow diagram illustrating method used to create the CFD model of roller pump.

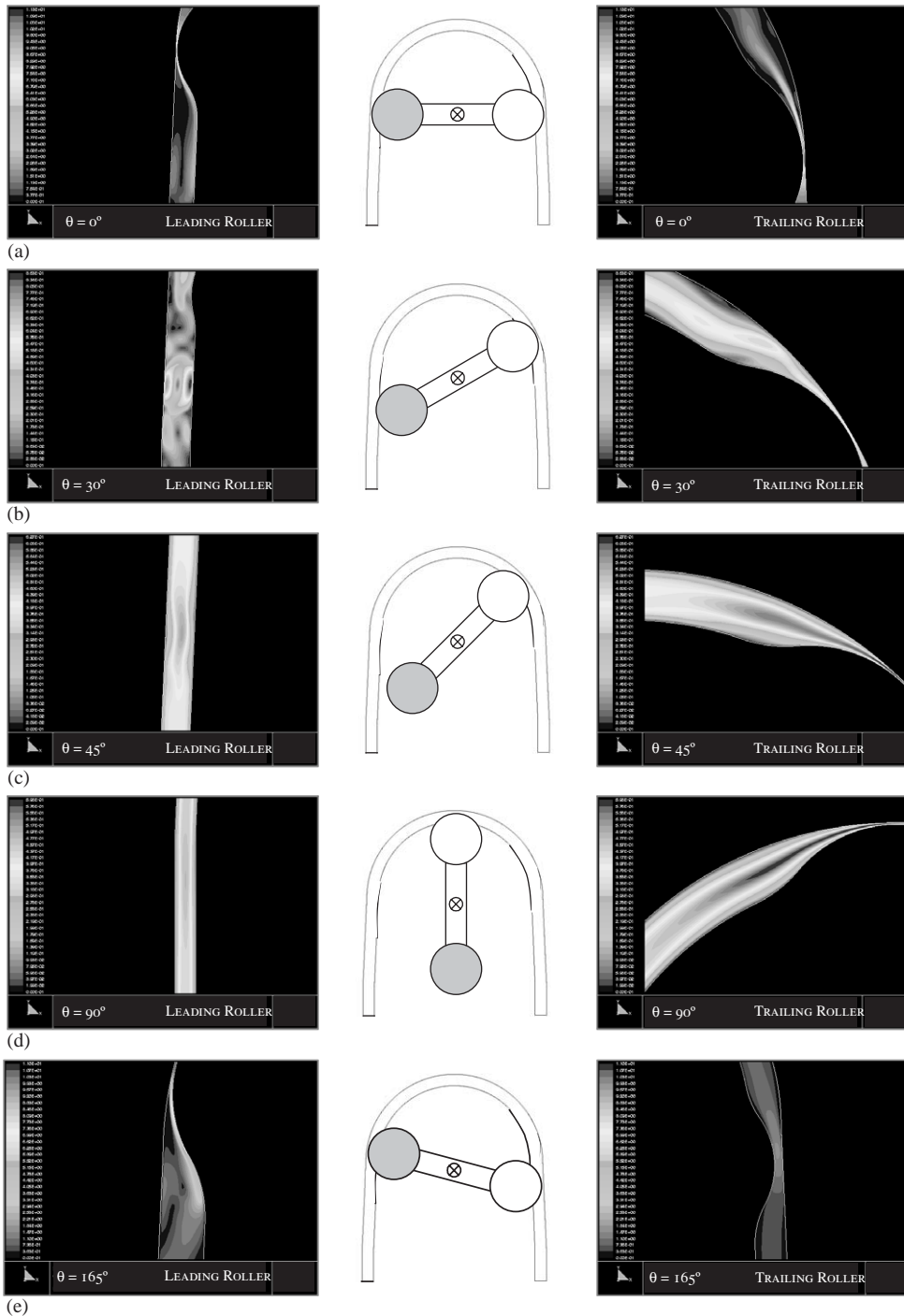


Fig. 3. (a) Velocity magnitude contours plotted between 0 and 11.31 m/s (maximum velocity) of the flow field near the rollers when $\theta = 0^\circ$. On the left is the flow near the leading roller and on the right is the flow near the trailing roller. (b) Velocity magnitude contours of the flow field near the rollers when $\theta = 30^\circ$, plotted between 0 and the maximum velocity of 0.87 m/s. On the left is the flow near the leading roller and on the right is the flow near the trailing roller. (c) Velocity magnitude contours of the flow field near the rollers when $\theta = 45^\circ$, plotted between zero and the maximum velocity of 0.63 m/s. On the left is the flow near the leading roller and on the right is the flow near the trailing roller. (d) Velocity magnitude contours of the flow field near the rollers when $\theta = 90^\circ$, plotted between zero and the maximum velocity of 0.60 m/s. (e) Velocity magnitude contours of the flow field near the rollers when $\theta = 165^\circ$, plotted between zero and the maximum velocity of 11.31 m/s. On the left is the flow near the leading roller and on the right is the flow near the trailing roller.

and the wall is very small ($= 1$ mm). Flow separation regions are also observed downstream of both rollers. This is the most dangerous position, which generates the maximum pressure drop, or resistance of the whole cycle. Then at $\theta = 30^\circ$, the leading roller is moving away from the wall, the flow is recovering near the leading roller, while a small flow separation region still exists just downstream of the trailing roller. The maximum velocity drops to 0.87 m/s. As the rollers continue to move to $\theta = 45^\circ$, the leading roller becomes detached from the wall, while the trailing roller is still squeezing the tube. The flow separation zone disappears, and the maximum velocity further decreases to 0.63 m/s. Then at $\theta = 90^\circ$, the rollers turn into a vertical position. The flow far away from the roller almost recovers to its undisturbed Poiseuille flow state, with a maximum velocity of 0.60 m/s. This is still much higher than the inlet velocity of 0.35 m/s. Finally, as the rollers move into position $\theta = 165^\circ$, both rollers start to squeeze the wall again, and the maximum velocity near the leading roller increases sharply back to 11.31 m/s. A large zone of flow separation is re-established downstream of the leading roller, and then the whole pattern then starts to repeat itself from $\theta = 180^\circ$ (i.e. $\theta = 0^\circ$) again. Note that the trailing roller becomes the leading one as it passes through 90° .

5.2. Wall shear stress

Fig. 4 shows the variation of the shear stress along the inner wall of the pump boot with varying roller position, θ (144° – 216°). As for the velocity magnitude, the peak value of the shear stress is seen with the leading roller in the horizontal position, $\theta = 0^\circ$ (i.e. $\theta = 180^\circ$).

A plot of peak shear stress along the whole length of the inner and outer walls for one full rotation is shown in Fig. 5. The peak shear stress is defined as the maximum shear stress at any point along the length of the tube for that particular time step (Δt). The plot shown starts at $\theta = 90^\circ$ and ends at 270° (half rotation). As the two rollers have identical shapes, the pattern repeats itself after 180° . The results show that the blood experienced nearly 8% higher shear stresses at the inner wall (994 N/m^2) compared to the outer wall (923 N/m^2) and therefore the remainder of the paper presents the inner wall stresses (inner 994 N/m^2 , outer 923 N/m^2). The significant shear stresses occur from $\theta = 144^\circ$ to 216° , as marked on the graph. It is noted that a sharp peak of shear stress occurs at $\theta = 180^\circ$. This is the position when both rollers are almost occluding the tube. There is a decrease in the volume of the tube as the second roller makes contact. Because the fluid is incompressible, the pressure between the rollers becomes very high and the fluid is driven through the narrow gaps very fast (as shown in Fig. 3). As a result, there exists a very thin boundary layer with high-velocity gradient, thus giving rise to a sharp peak of shear stress.

In fact, the computed peak shear stress is limited by the numerical resolution near the boundary layer; the actual value experienced by the blood cells may be even higher in this region.

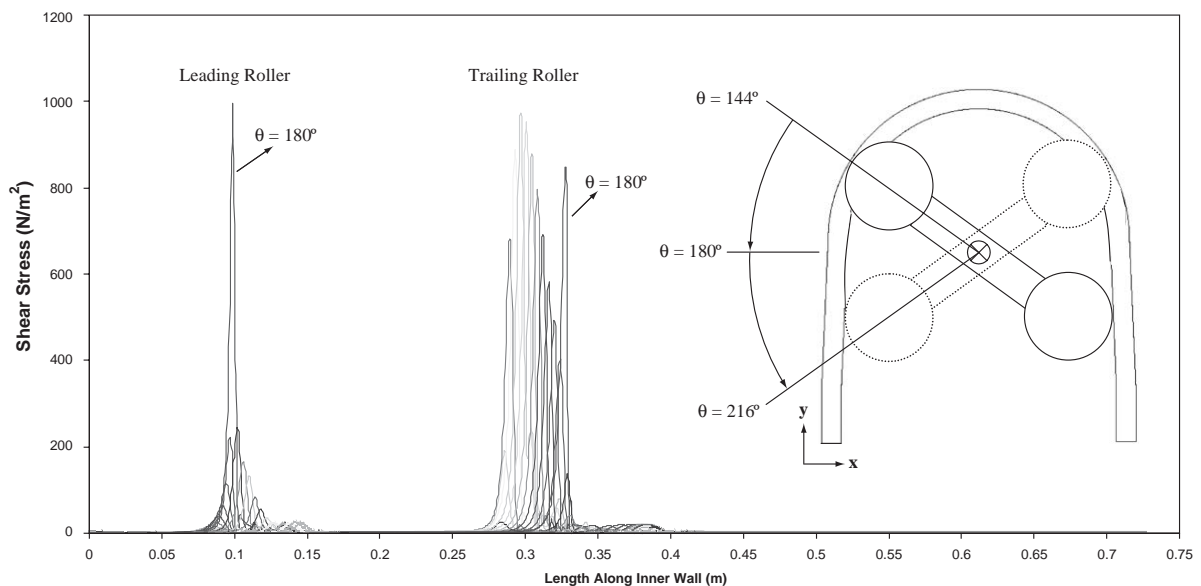


Fig. 4. Wall shear stress distribution along the arc length of the inner wall: five distributions are plotted at every 12 degrees from $\theta = 144^\circ$ to 216° .

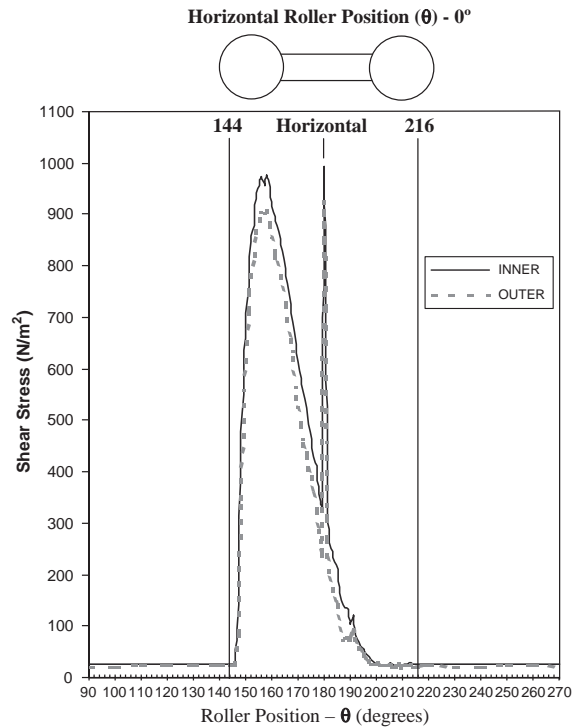


Fig. 5. The peak wall shear stress τ_w distributed along the inner (solid) and outer (dashed) walls during a half rotation.

6. Discussion

Cardiopulmonary bypass technology has not benefited from a large amount of CFD research because most of the current equipment was designed before CFD became widely available. Most of the CFD modelling carried out in the CPB field has focused on the centrifugal pump. Miyazoe et al. (1998, 1999), concluded that CFD could be a useful tool for developing blood pumps, but no direct comparisons between hemolysis tests and visualization tests were actually performed. Work reported by Pinotti and Rosa (1995), Nishida et al. (1999) and Takiura et al. (1998), focused on centrifugal pumps. Takiura et al. (1998) compared a selection of their CFD results with hemolysis tests and concluded that they were consistent. Although it is hard to draw comparisons, all the researchers found CFD to be valuable tool for developing blood pumps. This is one of the main aims of carrying out CFD analysis of the roller pump.

6.1. Wall shear stress

Blood experiences higher shear stresses at the inner wall than at the outer wall. This is because the velocity profile is more skewed towards the inner wall due to centrifugal force, and gives rise to a higher gradient. Two regions were observed during each rotation where increased shear stresses were predicted. The first occurred between $\theta = 144^\circ$ and 216° at either side of the horizontal roller position ($\theta = 180^\circ$). The second occurs at the either side of $\theta = 0^\circ$.

In order to understand the mechanism causing the high shear stresses several parameters were considered. These parameters have been plotted in Fig. 6. The peak shear stress, the occlusion of the leading roller, the average blood flow velocity at the outlet boundary of the model, the occlusion of the trailing roller, and the pressure drop across the pump boot were all plotted against roller position ($\theta = 144^\circ$ – 216°). The outlet flow velocity generated by the pump is actually pulsatile, varying from 0.71 m/s at $\theta = 168^\circ$ to 0.10 m/s at $\theta = 202^\circ$. This is a phenomenon seen in the clinical environment, although the roller pump is considered to deliver continuous flow in comparison to the beating heart (Wright, 1995). The pulse shown in the CFD results is both visible to the naked eye and evident on the integrated Tyco pressure gauge at the outlet of the pump boot. The numerical results allow us to look closely at a specific part of the rotation. Fig. 6 shows that the outlet flow velocity correlates with the peak shear stress to some extent.

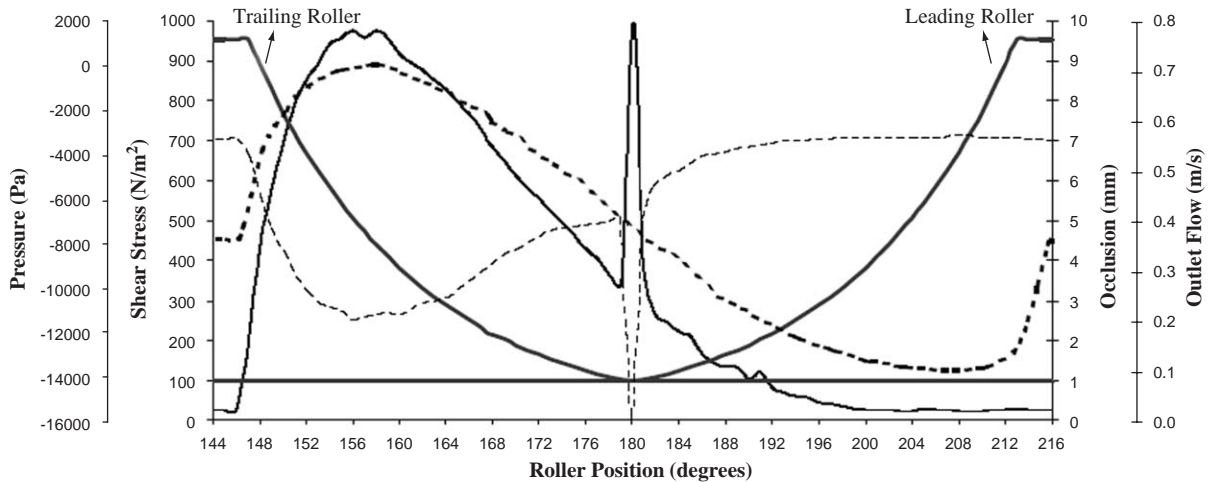


Fig. 6. The distribution of the peak shear stress (thin solid), rollers (thick solid), pressure (thin dotted) and the outlet flow velocity (thick dashed) plotted between $\theta = 144^\circ$ and 216° .

Table 1
Published threshold shear stresses for blood damage

	Threshold value (N/m ²)	Exposure time (s)	Type of exposure	Reference
1	150	120	Concentric cylinder viscometer	Leverette et al. (1972)
2	300	120	Concentric cylinder viscometer	Nevaril et al. (1968)
3	250	240	Concentric cylinder viscometer	Sutera and Mehrjardi (1975)
4	50-100	9000	Concentric cylinder viscometer	Sutera et al. (1972)
5	400	approx. 1×10^{-6}	Jet	Sallam and Hwang (1984)
6	450	approx. 1×10^{-5}	Pulsating gas bubble	Rooney (1970)
7	560	approx. 1×10^{-5}	Oscillating wire	Williams et al. (1970)

The increased pressure drop coincides exactly with the regions where both rollers are in contact with the pump tubing. This is reflected in Fig. 6 where the occlusion of the leading roller and trailing roller converge to 1 mm at 180° . This pressure drop increase is caused by an increased resistance as two rollers are almost in contact with the pump tubing, while our inlet flow rate is kept constant.

It is clear from this simulation that reducing the amount of time two rollers simultaneously occlude the tubing will reduce the blood exposure to shear stress significantly and consequently the blood damage caused. These findings can be used as an important design criterion for the re-design of the roller pump.

6.2. Blood damage prediction

In order to predict the blood damage, it is necessary to define a threshold shear stress value leading to blood cell damage. However, it is not clear from the published literature, see Table 1, what threshold shear stress value to apply for blood damage prediction. Clearly, the threshold shear stress is related to exposure time and the method that was used to expose blood to shear stress. Here we make an initial attempt to estimate the blood damage from the CFD simulations.

The exposure time for the CFD model is the time between each result file examined, which was 3.44×10^{-3} s. This value is an approximation, as some cells will be caught in the recirculation regions, thus increasing the exposure time. The other assumptions in our blood damage prediction include:

- (i) all damaging shear stress will occur at the wall;
- (ii) this shear stress will only damage the layer of cells nearest the wall;
- (iii) the shear stress from the 2-D model will be applied to the 3-D pump boot wall;
- (iv) all cells exposed to damaging shear stresses will be lysed.

Experiments (5–7) in Table 1 with the most comparative exposure times to the CFD model involved little or no interaction between the blood and a solid surface. The other experiments have longer exposure times and involve surface contact. The surface shear stress in the current model is similar to the experiments whereby blood was exposed to shear stress in a concentric cylinder viscometer (see experiments 1–4, Table 1). The theoretical blood damage was calculated using a range of threshold shear stresses. This range incorporated the experimentally derived thresholds for both short exposure time experiments and the surface contact experiments. The shear stresses above each threshold value were marked. There were two main regions of interest during the rotation, which were identified using Fig. 4 (see inset in Fig. 7). Fig. 7(a) focuses on the first peak seen during the rotation in Fig. 4, while Fig. 7(b) focuses on the second peak. The shear stresses above a range of thresholds were then examined. Fig. 7 shows the results with the threshold set at 150 N/m² (y-axis begins at 150 N/m²). We also carried out the blood damage analysis with the threshold shear stress set at 300, 400 and 560 N/m², respectively.

The amount of free haemoglobin released due to the lysis of cells at the wall can be estimated from the rate of change of plasma haemoglobin $\Delta p\text{Hb}$ (mg/dl s) using Eq. (3),

$$\Delta p\text{Hb} = \frac{V_d \Delta r_{\text{Hb}}}{V_t t_{\text{rev}}}, \tag{3}$$

where Δr_{Hb} is the mass concentration of haemoglobin in whole blood, V_t is the total volume of blood in the system, t_{rev} is the time taken per 360° roller revolution, and V_d is the approximate volume of the layer of blood (one cell deep) exposed to damaging shear stresses. This volume is calculated from

$$V_d = \sum_{\theta=0^\circ}^{360^\circ} L_\theta [\pi(r_1^2 - (r_1 - R_{\text{rbc}})^2)], \tag{4}$$

where L_θ is the length of cells along the pump boot wall exposed to damaging shear stresses during that particular degree of rotation, θ . L_θ is directly related to the exposure time and can be calculated from Fig. 7; r_1 is the radius of the tube and R_{rbc} is the diameter of a red blood cell, as shown in Fig. 8.

The threshold shear stress, the predicted volume of blood damaged per revolution and the rate of change of plasma haemoglobin are listed in Table 2. These results can be compared to the experimental value for rate of change of plasma haemoglobin found using horse blood in an experimental circuit that consisted of a roller pump and a reservoir connected by 1/4 inch surgical PVC tubing. The experiment was run for 40 min with the plasma haemoglobin levels being measured every 10 min. Mulholland et al. (2000) concluded that the rate of change of plasma haemoglobin was 2.04×10^{-4} mg/dl/s. It has been shown that as horse blood mimics human blood in all essential haematological aspects (Mulholland et al., 2000), this value is valid for human blood.

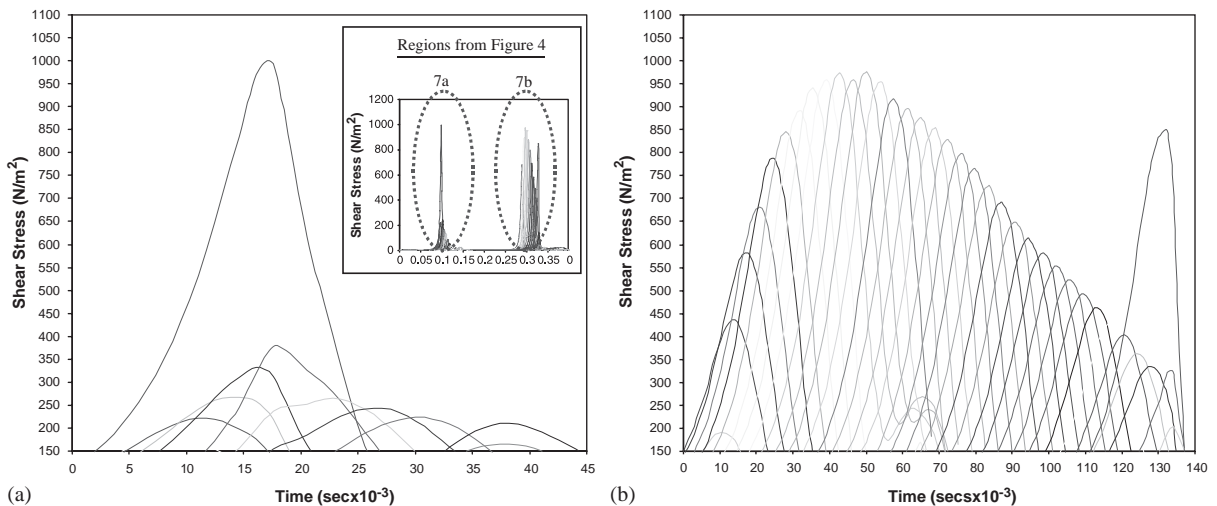


Fig. 7. Focus on the two regions (a and b) during one rotation where blood is exposed to shear stresses above the threshold value.

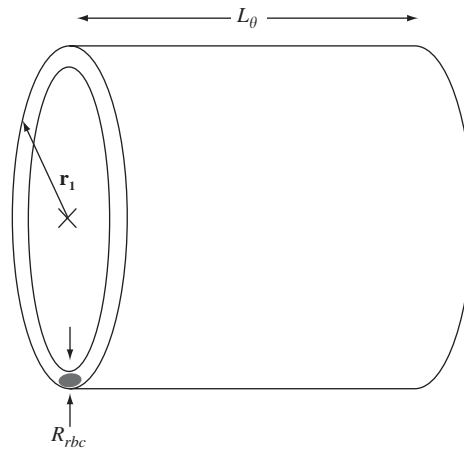


Fig. 8. Schematic diagram showing geometrical aspects of the wall layer.

Table 2
Hypothetical blood damage prediction for various threshold shear stresses

Hypothetical threshold shear stress (N/m^2)	Volume of blood damaged per revolution (dl)	Rate of change of plasma haemoglobin (mg/dl s)
150	1.49×10^{-7}	4.00×10^{-4}
300	1.21×10^{-7}	3.26×10^{-4}
400	1.17×10^{-7}	3.13×10^{-4}
560	1.08×10^{-7}	2.90×10^{-4}

As the hypothetical threshold value is increased, the theoretical rate of change of plasma haemoglobin gets closer to the experimental value. When the predicted blood damage results are considered alongside the previous work (Table 1) it is suggested that the exposure time is more important than surface contact. It should be noted that the role of accumulated sub-lethal damage is also very important. However, in our preliminary study, this has not yet been considered.

The most comprehensive blood damage prediction work to date has been carried out by Bludszweit (1995b), where particle tracking was used to predict damage but made no comparison to experimental values. One way to reduce the number of approximations and increase the accuracy of the theoretical value would be to use particle tracking. By doing this the Bludszweit model could be applied to predict the blood damage and the results could be compared not only to the experimental results but also the more basic model used here. Particle tracking may also facilitate the prediction of sub-lytic damage. Indeed, a particle tracking using Lagrangian integral of stress and exposure time over the population of red cells as they travel from flow inlet to outlet has been used by Ramstack et al. (1979). However this approach is not used here as the software used does not currently facilitate the combination of the deforming mesh model and particle tracking. Further work should clearly take this issue into consideration. Another way to increase the accuracy of the prediction would be to establish the exact blood lysis in these conditions.

7. Conclusions

A time-dependent moving boundary CFD model was used to gain an understanding of the fluid dynamics of the blood flow inside a roller pump used for cardiopulmonary bypass. It is found that the highest shear stresses occur for the period when the roller pump boot is simultaneously occluded in two places. Eliminating or reducing this period of double occlusion will reduce the shear stress related blood damage caused by the roller pump. This conclusion will be used as a starting point for future work on the re-design of the arterial roller pump. The rate of blood damage of 4.00×10^{-4} mg/dl s is predicted using a simple model showed an acceptable comparison to the experimental findings (2.04×10^{-4} mg/dl s) of Mulholland et al. (2000). This blood damage prediction model could be validated by in vitro experiment, establishing a threshold shear stress value for the modeled exposure conditions and exposure times. In the

future this information combined with the use of particle tracking would allow other models to be compared, as well as the development of a more accurate blood prediction model.

References

- Anderson, J.B., Wood, H.G., Allaire, P.E., Bearnson, G., Khanwildar, P., 2000. A computational flow study of the CF3 blood pump. *Artif Organs* 24, 377–385.
- Bernstein, E.F., Blackshear Jr., P.L., Keller, K.H., 1967. Factors influencing erythrocyte destruction in artificial organs. *American Journal of Surgery* 114, 126–138.
- Blackshear, P.L., Dorman, F.D., Steinbach, J.H., 1965. Some effects that influence hemolysis. *Transactions—American Society for Artificial Internal Organs* 11, 112–117.
- Bludszuweit, C., 1995a. Three-dimensional numerical prediction of stress loading of blood particles in a centrifugal pump. *Artificial Organs* 19, 590–596.
- Bludszuweit, C., 1995b. Model for general blood damage prediction. *Artificial Organs* 19, 583–589.
- Bluestein, M., Mockros, L.F., 1969. Hemolytic effects of energy dissipation in flowing blood. *Medical & Biological Engineering* 7, 1–16.
- Fung, Y.C., 1993. In *Biomechanics, Mechanical Properties of Living Tissues*, Second ed. Springer, Berlin.
- Hansbro, S.D., Sharpe, D.A.C., Catchpole, R., 1999. Hemolysis during CPB: an in vivo comparison of standard roller pumps, non-occlusive roller pumps and centrifugal pumps. *Perfusion* 14, 3–10.
- Huang, C.R., Fabisiak, W., 1978. A rheological equation characterizing both the time dependent and the steady state viscosity of whole human blood. *American Institute of Chemical Engineers—Symposium Series*, pp. 19–21.
- Leverette, L.B., Hellums, J.D., Alfrey, C.P., Lynch, E.C., 1972. Red blood cell damage by shear stress. *Biophysical Journal* 12, 257–273.
- Miyazoe, Y., Sawairi, T., Ito, K., Konishi, Y., Yamane, T., Nishida, M., Asztalos, B., Masuzawa, T., Tsukiya, T., Endo, S., Taenaka, Y., 1999. Computational fluid dynamics analysis to establish the design process of a centrifugal blood pump: second report. *Artificial Organs* 23, 762–768.
- Miyazoe, Y., Sawairi, T., Ito, K., Konishi, Y., Yamane, T., Nishida, M., Masuzawa, T., Takiura, K., Taenaka, Y., 1998. Computational fluid dynamic analyses to establish design process of centrifugal blood pumps. *Artificial Organs* 22, 381–385.
- Mulholland, J.W., Massey, W., Shelton, J.C., 2000. Investigation and quantification of the blood trauma caused by the combined dynamic forces experienced during cardiopulmonary bypass. *Perfusion* 15, 485–494.
- Nakamura, S., Ding, W., Smith, W., Golding, L., 1999. Numeric flow simulation for an innovative ventricular assist system secondary impeller. *American Society for Artificial Internal Organs* 45, 74–78.
- Nevaril, C.G., Lynch, E.C., Alfrey, C.P., Hellums, J.D., 1968. Erythrocyte damage and destruction induced by shearing stress. *Journal of Laboratory Clinical Medicine* 71, 784–790.
- Nishida, M., Asztalos, B., Yamane, T., Masuzawa, T., Tsukiya, T., Endo, S., Taenaka, Y., Miyazoe, Y., Ito, K., Konishi, Y., 1999. Flow visualization study to improve hemocompatibility of a centrifugal blood pump. *Artificial Organs* 23, 697–703.
- Pinotti, M., Rosa, E.S., 1995. Computational prediction of hemolysis in a centrifugal ventricular assist device. *Artificial Organs* 19, 267–273.
- Ramstack, J.M., Zuckerman, L., Mockros, L.F., 1979. Shear-induced activation of platelets. *Journal of Biomechanics* 12, 113–125.
- Rooney, J.A., 1970. Hemolysis near an ultrasonically pulsating gas bubble. *Science* 16, 869–871.
- Sallam, A.M., Hwang, N.H., 1984. Human red blood cell hemolysis in a turbulent shear flow: contribution of Reynolds shear stresses. *Biorheology* 21, 783–797.
- Sukumar, R., Athavale, M., Makhijani, V., Przekwas, A., 1996. Application of computational fluid dynamics techniques to blood pumps. *Artificial Organs* 20, 529–533.
- Sutera, S.P., Mehrjardi, M.H., 1975. Deformation and fragmentation of human RBC in turbulent shear flow. *Biophysical Journal* 15, 1–10.
- Sutera, S.P., Croce, P.A., Mehrjardi, M.H., 1972. Hemolysis and subhemolytic alterations of human RBC induced by turbulent shear flow. *Transactions—American Society for Artificial Internal Organs* 18, 335–341.
- Takahama, T., Kanai, F., Hiraishi, M., Onishi, K., Yamazaki, Z., Suma, K., Asano, K., Kazama, M., 1985. Long-term non-heparinized left heart bypass (LHB): centrifugal pump or roller pump. *Transactions—American Society for Artificial Internal Organs* 31, 372–376.
- Takiura, K., Masuzawa, T., Endo, S., Wakisaka, Y., Tatum, E., Taenaka, Y., Takano, H., Yamane, T., Nishida, M., Asztalos, B., Konishi, Y., Miyazoe, Y., Ito, K., 1998. Development of design methods of a centrifugal blood pump with in vitro tests, flow visualization, and computational fluid dynamics: results in hemolysis tests. *Artificial Organs* 22, 393–398.
- Williams, A.R., 1973. Shear-induced fragmentation of human erythrocytes. *Biorheology* 10, 303–311.
- Williams, A.R., Hughes, D.E., Nyborg, W.L., 1970. Hemolysis near a transversely oscillating wire. *Science* 16, 871–873.
- Wright, G., 1995. The assessment of pulsatile blood flow. *Perfusion* 10, 135–140.
- Yarborough, K.A., Mockros, L.F., Lewis, F.J., 1966. Hydrodynamic hemolysis in extracorporeal machines. *Journal of Thoracic and Cardiovascular Surgery* 52, 550–557.